Journal of Alloys and Compounds, 203 (1994) 169–176
JALCOM 879

Structure and magnetic properties of Fe_4N–Fe alloys produced by mechanical milling

Kyu-Jin Kim, Kenji Sumiyama, Hideya Onodera and Kenji Suzuki
Institute for Materials Research, Tohoku University, Katahira 2-1-1, Aoba-ku, Sendai 980 (Japan)

(Received June 17, 1993)

Abstract

The structural changes and magnetic properties of mechanically milled Fe_4N–Fe and γ'-Fe_4N alloys have been investigated. During the initial stage of milling, the γ'-Fe_4N phase is transformed to the b.c.t. structure of the α-Fe type owing to a stress-induced martensitic transformation. The initial increase in saturation magnetization (σ) is also due to the structure change of the γ'-Fe_4N phase from f.c.c. to b.c.t. and the volume expansion of the b.c.t. unit cell. After annealing well-milled Fe_4N–Fe alloys, the γ'-Fe_4N phase is formed above 473 K and the α''-$Fe_{16}N_2$ phase partially appears together with γ'-Fe_4N above 673 K, causing an increase in σ. However, only the α-Fe phase is retained above 873 K as a result of N atoms evaporating from the Fe matrix.

1. Introduction

Ferromagnetic iron nitride has attracted much attention as a candidate material for magnetic recording heads and magnetic recording media [1, 2] because of its high magnetic flux and good corrosion resistance in comparison with pure iron. Recently, Sugita *et al.* [3] succeeded in obtaining the α''-$Fe_{16}N_2$ phase with a high magnetic flux density (B_s) of about 2.8–3.0 T by using the molecular beam epitaxy (MBE) method. However, the mass production of such materials has been desired for various technical applications.

Mass production of non-equilibrium phases such as amorphous [4, 5], quasi-crystalline [6] and nanocrystalline [7, 8] materials can be achieved by mechanical milling techniques. In this paper we synthesized γ'-Fe_4N in an NH_3 gas flow atmosphere and then studied the structure and magnetic properties of Fe_4N–Fe alloyed powders prepared by a vibrating ball mill as a function of milling time.

2. Experimental procedures

The synthesis of γ'-Fe_4N was carried out by nitrization at 823 K in an NH_3 gas flow atmosphere [9]. γ'-Fe_4N and α-Fe powders were mixed to give the desired compositional ratio of γ'-Fe_4N:α-Fe = 1:4 for mechanical alloying (MA), while only γ'-Fe_4N powder was supplied for mechanical grinding (MG). A vibrating ball mill was operated at a frequency of 9.6 Hz under an N_2 gas atmosphere at room temperature. The powder-to-ball weight ratio was 1:7. The milling processes were stopped and the vial opened in a glove-box to take out small amounts of samples for various analyses. The well-milled alloy powders were subsequently annealed at various temperatures in a vacuum of about 5×10^{-5} Torr. The milled and annealed powders were characterized by means of X-ray diffraction (XRD) with Cu Kα radiation and Mössbauer spectroscopy at room temperature. Their microstructures were observed by transmission electron microscopy (TEM) and the magnetic properties of the milled alloys were measured using a vibrating sample magnetometer (VSM). The chemical compositions were analyzed by inductively coupled plasma (ICP) analysis and the He carrier fusion–thermal conductivity method (Table 1).

TABLE 1. Chemical analyses of Fe_4N–Fe alloy powders after selected milling times. The results for Fe and Cr have been obtained by ICP analysis and those for O and N by the He carrier fusion method

	Milling time (h)	Chemical composition (wt.%)			
		Fe	N	Cr	O
Fe_4N–4Fe	0	95.7	3.05	<0.01	0.37
	300	95.6	3.18	0.02	1.28
Fe_4N	0	93.8	5.90	–	0.76
	300	91.7	4.83	0.77	1.26

SSDI 0925-8388(93)00879-4

3. Results

3.1. Fe_4N–4Fe alloy

Figure 1 shows the XRD patterns of mechanically alloyed (MA) Fe_4N–4Fe powders as a function of milling time. During the initial stage of MA the relative intensities of the Bragg diffraction peaks of f.c.c. γ'-Fe_4N decrease, while those of the α-Fe type increase rapidly. After 300 h of MA only the peaks of the α-Fe type are observed and their widths become large. However, it is noteworthy that the first peak of the α-Fe type is asymmetric after 50 h of MA and gradually becomes asymmetric with a further increase in milling time, indicating that nitrogen atoms are arranged regularly in the initially formed α-Fe-type phase and distributed randomly by milling. This result is consistent with the Mössbauer spectra as a function of milling time as shown in Fig. 2. The observed curve of the as-mixed powder is composed of three "sextets" with a relative volume ratio of 4:3:1 for α:γ'_2:γ'_1, where the γ'-Fe_4N phase contains two Fe sites γ'_2 and γ'_1. After 50 h of MA the intensities of the γ'-Fe_4N phase are rapidly

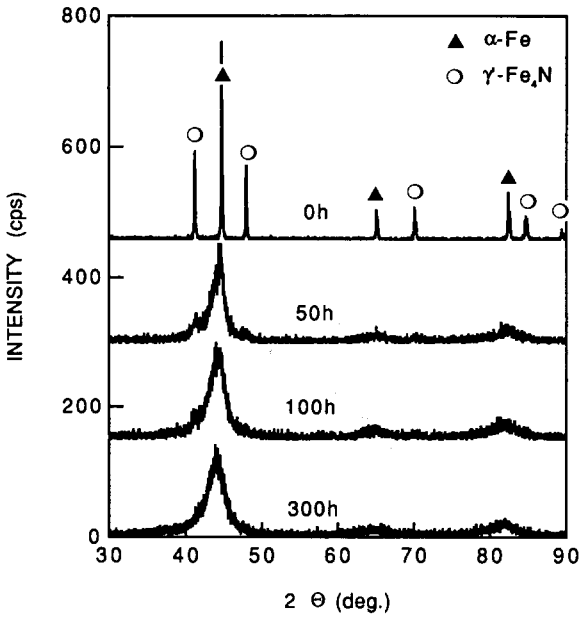

Fig. 1. XRD patterns of Fe_4N–4Fe alloy powders as a function of milling time.

TABLE 2. Mössbauer parameters for Fe_4N–4Fe as a function of milling time at room temperature; H_i is the magnetic hyperfine field, δ the isomer shift and ΔW the linewidth

Material	Component	H_i (kOe)	δ (mm s^{-1})	ΔW (mm s^{-1})
0 h	γ_1'	341	0.14	0.430
	γ_2'	216	0.30	0.323
	α	329	0.00	0.215
50 h	γ_1'	343	0.05	0.299
	γ_2'	220	0.32	0.329
	α'	331	0.01	0.250
	α_1'	300	0.15	0.312
100 h	γ_1'	347	0.07	0.205
	γ_2'	215	0.34	2.666
	α'	334	0.01	0.282
	α_1'	300	0.16	0.326
300 h	α'	334	0.00	0.310
	α_1'	278	0.15	0.450

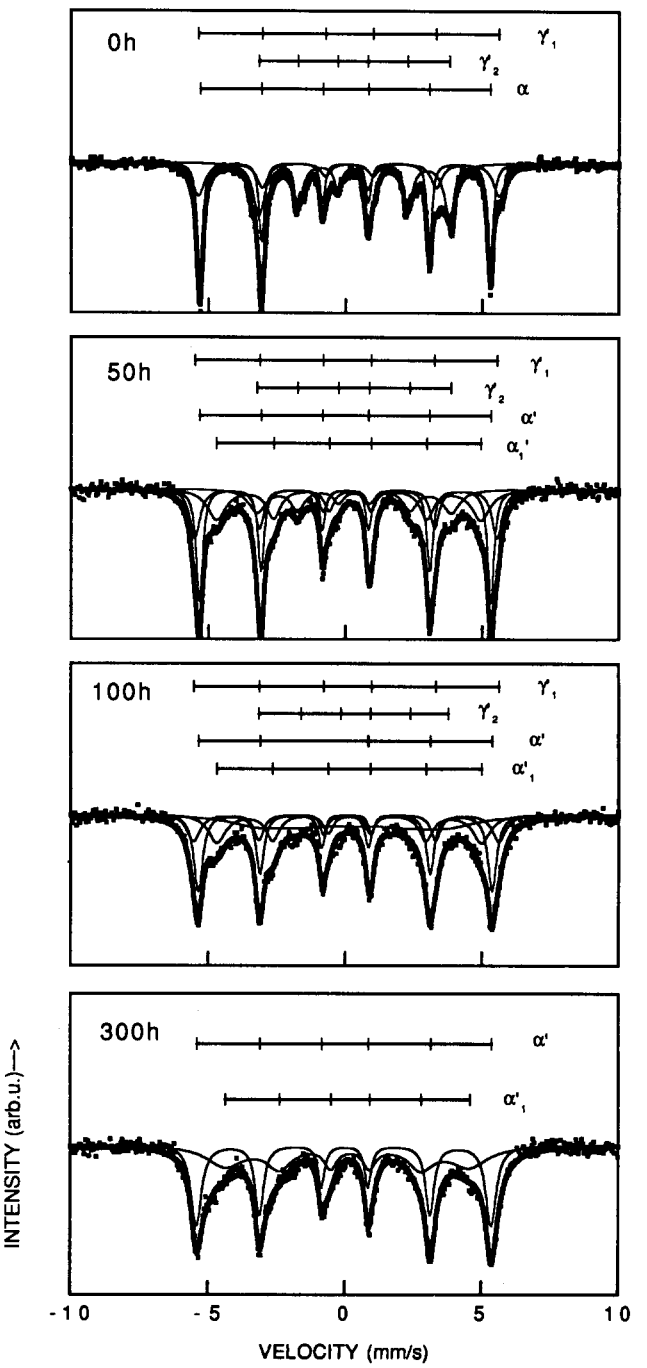

Fig. 2. Mössbauer spectra of Fe_4N–4Fe alloy powders as a function of milling time.

reduced, while new components of α' and α'_1 appear rapidly at the position of α and the intermediate position of γ'_2 and α. The intensities of α' and α'_1 increase and their halfwidths become large with a further increase in milling time. As listed in Table 2, the hyperfine fields of 300 and 331 Oe are ascribed to the Fe atoms whose first- and second-nearest octahedral interstitial sites are occupied by nitrogen atoms in the martensite phase [10, 11]. After 300 h of milling, only the α' and α'_1 spectra are observed, indicating a complete change to the b.c.t. structure.

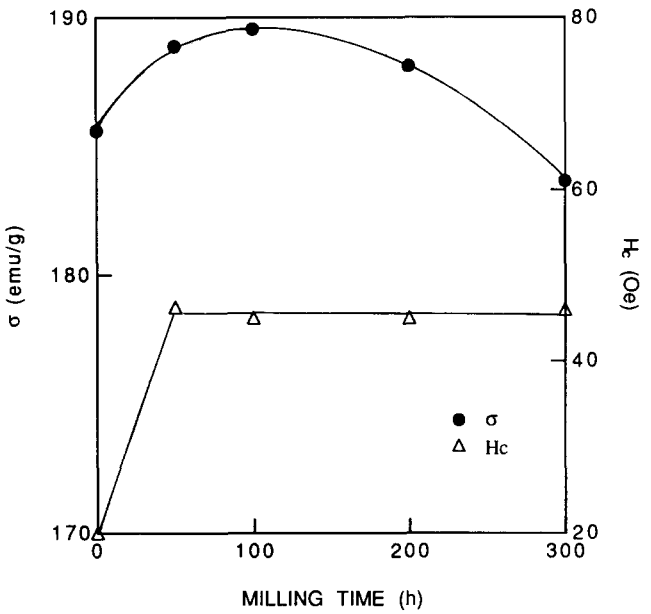

Fig. 3. Saturation magnetization σ and coercive force H_c of Fe_4N–4Fe alloy powders.

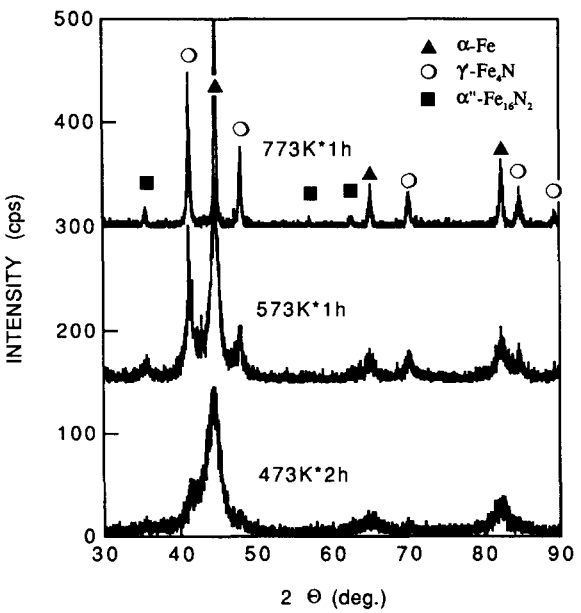

Fig. 4. XRD patterns of 300 h milled Fe_4N–4Fe alloy powders as a function of annealing temperature.

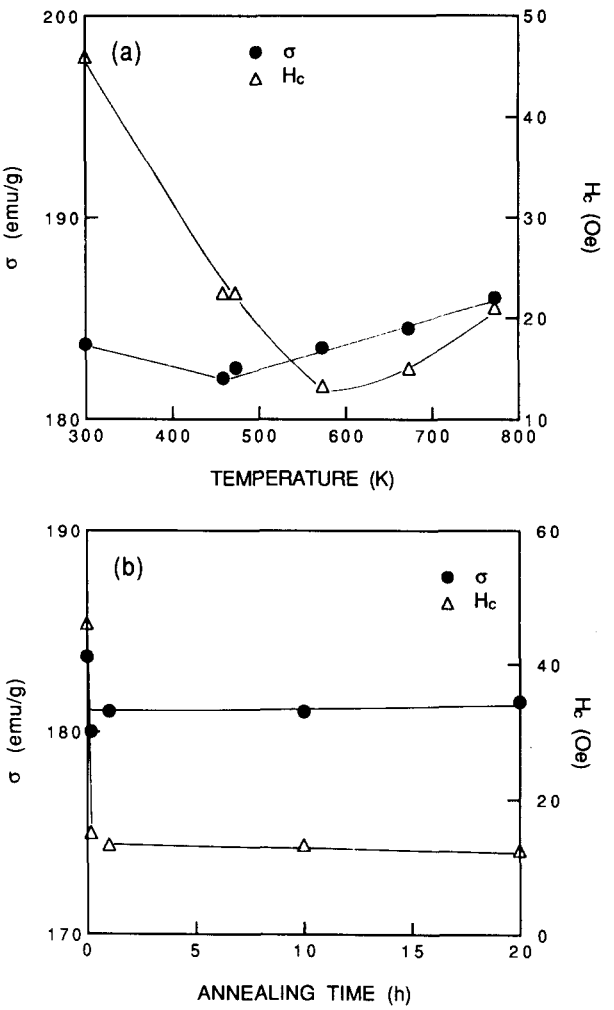

Fig. 5. Saturation magnetization σ and coercive force H_c of 300 h milled Fe_4N–4Fe alloy powders: (a) isochronal annealing for 1 h; (b) isothermal annealing at 573 K.

As shown in Fig. 3, the saturation magnetization (σ) increases slightly during the initial stage of milling and becomes almost constant until 200 h of MA. The increase in σ is due to the structural change from f.c.c. to b.c.t. in γ'-Fe_4N and the volume expansion caused by supersaturated N atoms in the b.c.t. phase. After 200 h of MA σ decreases with milling time. On the contrary, the coercive force (H_c) initially increases rapidly and then becomes almost constant. The initial increase in H_c is mainly due to the internal strain stored during milling.

Figure 4 shows the XRD patterns of alloy powders milled for 300 h as a function of annealing temperature. Below 433 K no phase change can be detected. Above 473 K γ'-Fe_4N precipitates from the b.c.t. phase of the α-Fe type in which N atoms are supersaturated. At 573 K the intensity ratio $I_{\gamma'(111)}/I_{\alpha(110)}$ is almost the same as that of the as-mixed powder. Above 673 K a new phase, which can be assigned to α''-$Fe_{16}N_2$, is additionally formed together with γ'-Fe_4N. With in-

creasing annealing temperature in Fig. 5(a) σ increases slowly between 573 and 773 K owing to grain growth and strain relaxation. However, H_c decreases rapidly even after annealing at 433 K and becomes almost constant between 473 and 773 K. This result indicates that the internal strain stored during milling is released even by low temperature annealing. In Fig. 5(b) the crystal growth during isothermal annealing at 573 K does not contribute to the decrease in H_c. The formation of α''-$Fe_{16}N_2$ results in an increase in σ, but we cannot quantitatively discriminate its contribution.

3.2. γ'-Fe_4N

Figure 6(a) shows the XRD patterns of mechanically ground (MG) f.c.c. γ'-Fe_4N powders as a function of milling time. After 20 h of MG the relative intensities of the Bragg diffraction peaks of the γ'-Fe_4N phase decrease, while new peaks of the α-Fe-type phase appear rapidly, as observed for mechanically alloyed Fe_4N–4Fe powders. The width of the first peak (110) of the α-Fe-type phase is small, indicating that the α-Fe-type

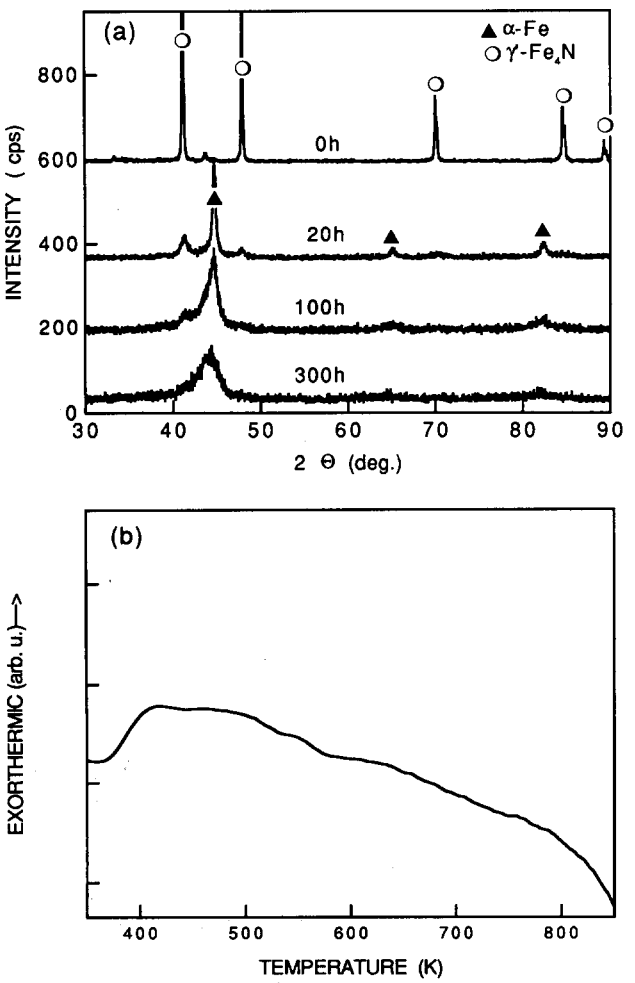

Fig. 6. (a) XRD patterns of γ'-Fe_4N powders as a function of milling time. (b) DSC traces of 300 h milled γ'-Fe_4N powder.

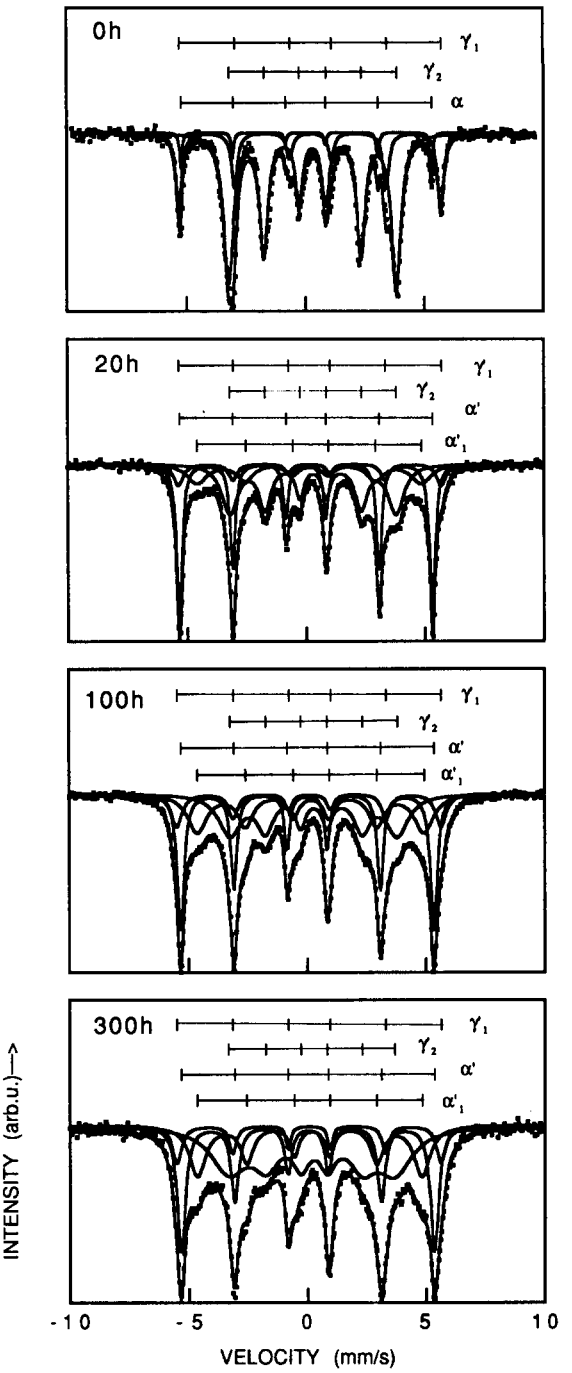

Fig. 7. Mössbauer spectra of γ'-Fe_4N powders as a function of milling time.

phase forms easily by applying a small amount of stress on γ'-Fe_4N powder. With a further increase in MG time the widths of the α-Fe-type peaks become large and then a broad amorphous-like pattern appears after 100 h of MG. Although this amorphous-like pattern has also been observed in the TEM image of a 300 h milled sample in our previous work [9], the differential scanning calorimetry (DSC) trace of the same milled powder heated at a rate of 20 K m^{-1} does not show

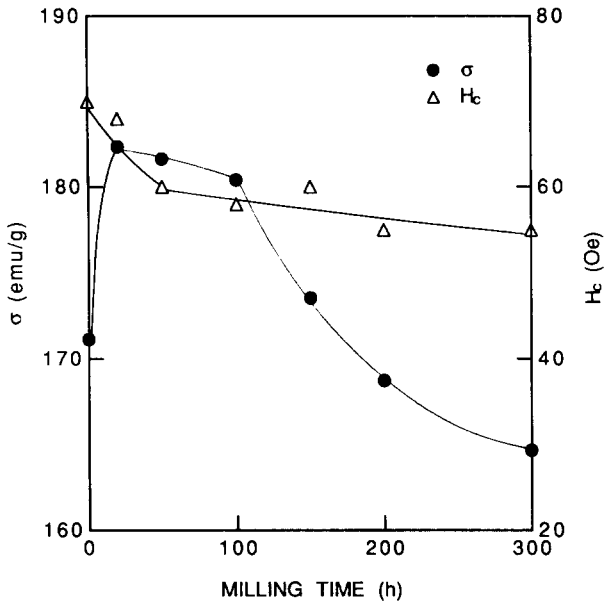

Fig. 8. Saturation magnetization σ and coercive force H_c of γ'-Fe_4N powders as a function of milling time.

sharp peaks but only a broad exothermic curve due to the precipitation of γ'-Fe_4N particles and their grain growth, as shown in Fig. 6(b). Figure 7 shows the Mössbauer spectra as a function of MG time. The spectrum of the as-nitrided sample consists mainly of the γ'-Fe_4N components γ'_1 and γ'_2 together with a small amount of the unnitrided α-Fe component α (volume fraction less than 8%). After 20 h of MG the intensity of γ'-Fe_4N is rapidly reduced, while new components α' and α'_1 appear rapidly. The hyperfine fields listed in Table 2 are the same as those of mechanically alloyed Fe_4N–4Fe powders. After 20 h of MG the width of the α' component is very small and similar to that of the α component of 0 h of MG. This is consistent with the XRD result in Fig. 6(a). However, the width of the α'_1 component is very large, indicating a marked distribution of the hyperfine field probably as a result of severe distortion caused by the nearest-neighbour N atoms. With a further increase in milling time the widths of the α' and α'_1 components become large and their intensities increase. However, even after 300 h of MG the volume fraction of the γ' component is about 20%, although the XRD patterns in Fig. 6(a) show only α-Fe-type peaks.

As shown in Fig. 8, the saturation magnetization (σ) initially increases and then decreases slowly after 100 h of MG. These results agree with those for mechanically alloyed Fe_4N–4Fe powders. On the other hand, the coercive force (H_c) initially decreases rapidly, in contrast with the result for mechanically alloyed Fe_4N–4Fe powders, and then becomes almost constant with a further increase in milling time.

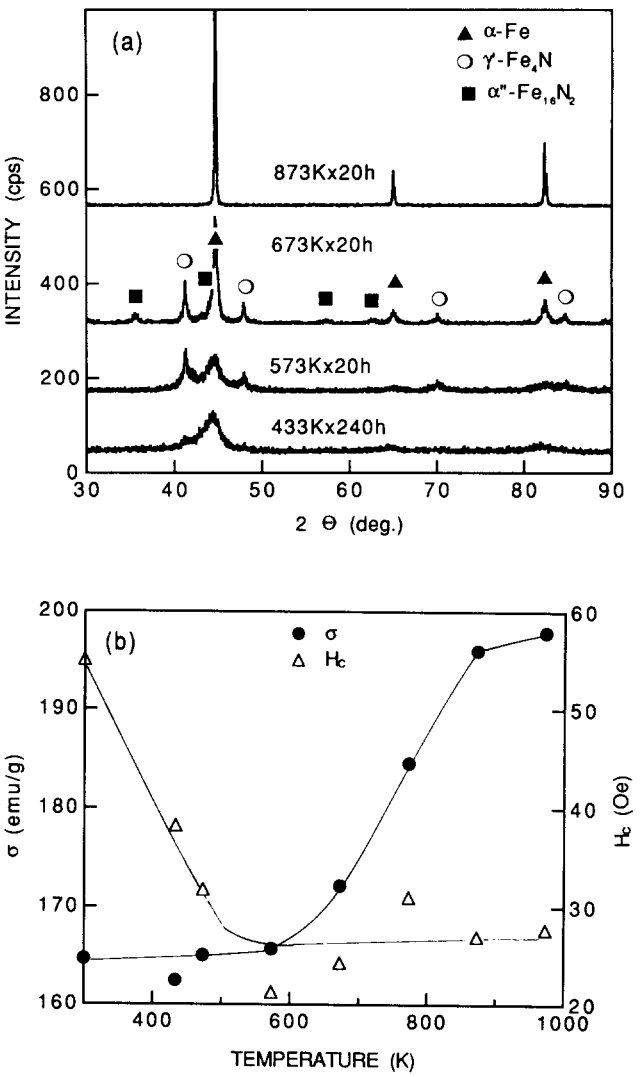

Fig. 9. (a) XRD patterns and (b) saturation magnetization σ and coercive force H_c of 300 h milled γ'-Fe_4N powders as a function of annealing temperature.

Figure 9(a) shows the XRD patterns of 300 h milled alloys as a function of annealing temperature. At 433 K α-Fe and γ'-Fe_4N are formed from the b.c.t. phase of the α-Fe type. At 673 K a new phase, which can be assigned to α''-$Fe_{16}N_2$, additionally appears together with the α-Fe and γ'-Fe_4N phases. The peak positions in the XRD pattern are consistent with Jack's results [12]. On the other hand, only the α-Fe phase is retained after annealing above 873 K. As shown in Fig. 9(b), σ increases until 873 K and then becomes almost constant above that temperature. This result indicates the vaporization of N atoms from the Fe matrix. As seen in Fig. 10, the Mössbauer spectrum demonstrates the presence of the α''-$Fe_{16}N_2$ phase; the hyperfine field of 457 kOe is larger than that of α-Fe (Table 3). The value is almost the same as that of α''-$Fe_{16}N_2$ determined by Sugita *et al.* [3].

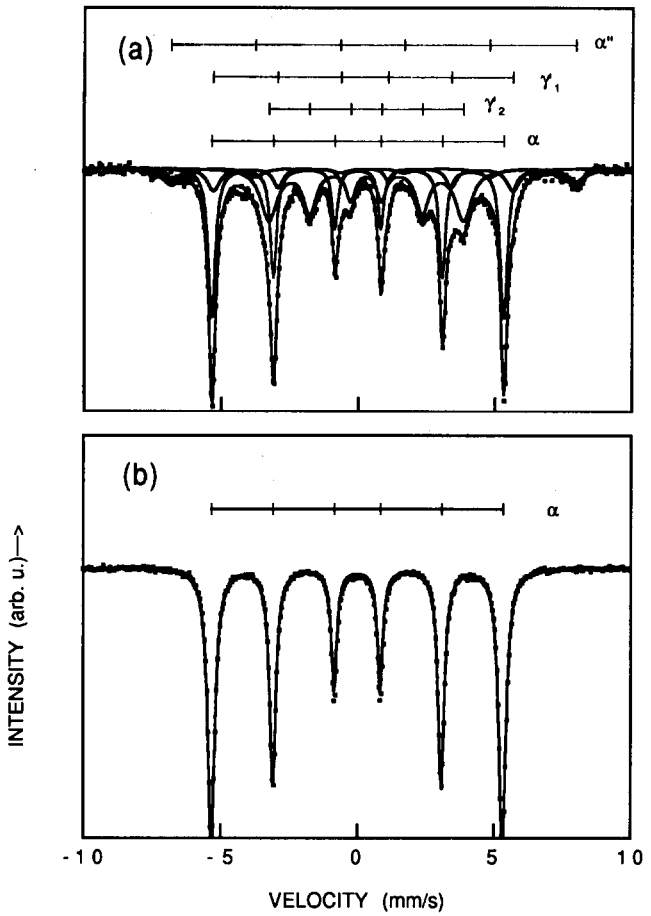

Fig. 10. Mössbauer spectra of 300 h milled γ'-Fe_4N powders at various annealing temperatures: (a) 673 K, 20 h; (b) 873 K, 20 h.

TABLE 3. Mössbauer parameters for Fe_4N as a function of milling time at room temperature; H_i is the magnetic hyperfine field, δ the isomer shift and ΔW the linewidth

Material	Component	H_i (kOe)	δ (mm s^{-1})	ΔW (mm s^{-1})
As nitrided	γ_1'	342	0.22	0.180
	γ_2'	219	0.30	0.337
	α	327	0.03	0.180
20 h	γ_2'	345	0.13	0.391
	γ_2'	217	0.30	0.443
	α'	330	0.00	0.247
	α_1'	297	0.17	0.330
100 h	γ_1'	345	0.09	0.356
	γ_2'	219	0.27	0.408
	α'	331	0.01	0.270
	α_1'	296	0.16	0.453
300 h	γ_1'	345	0.06	0.212
	γ_2'	218	0.22	0.653
	α'	331	0.02	0.270
	α_1'	294	0.14	0.399
673 K	γ_1'	336	0.14	0.434
	γ_2'	221	0.28	0.488
	α	331	0.01	0.220
	α''	458	0.30	0.370
873 K	α	331	0.00	0.214

4. Discussion

Although there is no significant change in N content in Fe_4N–4Fe and γ'-Fe_4N alloy powders during milling (see Table 1), most of the γ'-Fe_4N phase is initially transformed to the b.c.t. structure of the α-Fe type. This result indicates that the b.c.t. phase of the α-Fe type is easily formed by applying a small amount of stress on γ'-Fe_4N powder. The peak separation due to the tetragonal distortion is not apparent in the XRD patterns of Figs. 1 and 6(a). However, the (110) peak of the α-Fe-type phase is asymmetric, suggesting compositional inhomogeneity of the α-Fe-type phase or the formation of a new phase. As shown in Fig. 11, the peak between 43° and 45° for the 20 h milled powder, which almost corresponds to the (110) peak position of the pure α-Fe phase, can be divided into two Gaussian peaks after appropriate corrections for $K\alpha_2$ and instrumental broadening [13]. The low and high angle peaks correspond to (101) and (110) respectively of the b.c.t. phase transformed from the γ'-Fe_4N matrix. The positions of these peaks shift to the lower angle side with increasing milling time. Figure 12 shows that the planar distances of these peaks, d_{101} and d_{110}, increase almost linearly and become about 2.11 and 2.05 Å respectively after 300 h of MG. Using these values, we calculate the unit cell volume of this phase to be $V=a^2c=25.86$ Å^3. The lattice constants a and c of the Fe–N system vary linearly with increasing concentration of N [14, 15]:

$$a = 2.866 - 0.003x$$

$$c = 2.866 + 0.025x$$

$$c/a = 1.000 + 0.01x$$

where x is the atomic fraction of N.

According to these equations, the unit cell volume of the sample after 300 h of MG corresponds to a N incorporation of about 15 at.% in the octahedral interstitial sites of the α-Fe structure, while the N composition of 300 h milled $\gamma'Fe_4N$ is about 19 at.% (Table 1). This difference is mainly due to the amount of untransformed γ'-Fe_4N after 300 h of MG. With increasing N content in the martensite phase of Fe–N alloys, the lattice parameter of the a axis decreases and that of the c axis increases, while the a axis of the Fe–N system in the present work increases with increasing milling time. This result means that N atoms are randomly distributed over the octahedral interstitial sites. The transformations of γ'-Fe_4N during milling

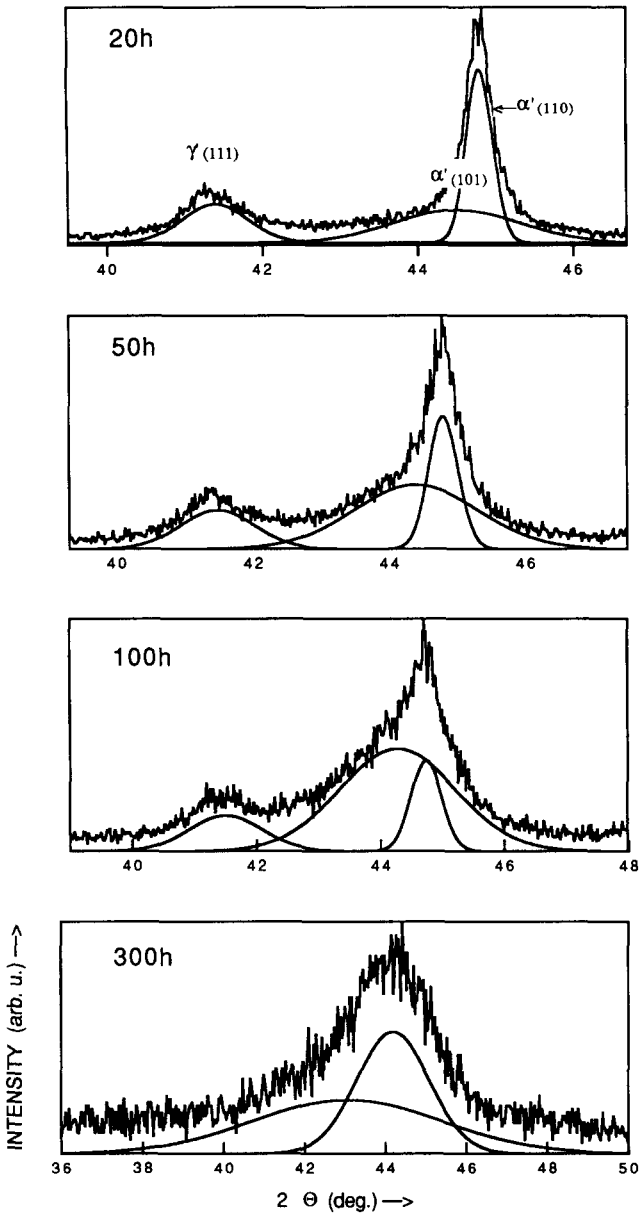

Fig. 11. Gaussian-fitting results of the first diffraction peak {110} of the α-Fe type as a function of milling time in XRD patterns of Fig. 6(a).

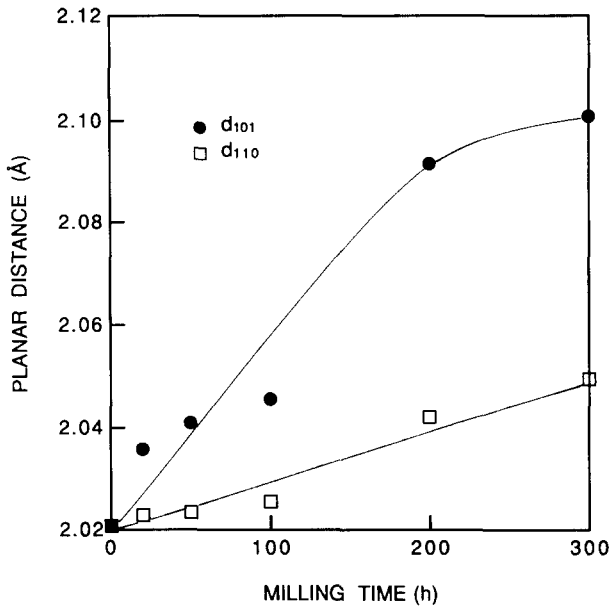

Fig. 12. Planar distances d_{101} and d_{110} as a function of milling time; d_{101} and d_{110} are the distances defined by the lower and higher angle peaks respectively in Fig. 11.

is similar to a stress-induced martensitic transformation via Bain's distortion mechanism [15]. In this model the f.c.c. unit cell is reconstructed into the b.c.t. structure and a phase transformation occurs on applying a small stress. The occurrence of a stress-induced martensitic transformation in Fe_4N–Fe alloys can be confirmed by the following evidence.

(1) As shown in Fig. 6(a), the new {110} peak of the α-Fe-type structure initially appears rapidly. The width is very small and can be divided into two peaks as shown in Fig. 11.

(2) During the initial stage of milling, the α' and α_1' components in Fig. 7 appear rapidly and the width of the α' component is very small. The α'_1 and α' components correspond to Fe atoms whose first- and second-nearest-neighbour sites are occupied by N atoms, because N atoms in Fe–N alloys are known to act as electron donors to the nearest Fe atoms [16, 17]. However, the width of the α'_1 component is much larger during the initial stage of milling than that of the α' component. This implies that the first-nearest-neighbour Fe atoms around N atoms are distorted markedly during the initial stage of milling. In fact, the size of the N atom is larger than that of the octahedral interstitial sites in the α-Fe structure. In order for those sites of the α-Fe phase to be occupied, their environment must be distorted. During the initial stage of the martensitic transformation, N atoms occupy mainly the $(0,0,\frac{1}{2})$ octahedral interstitial site of the c axis and then randomly diffuse into the $(0,\frac{1}{2},\frac{1}{2})$ and $(\frac{1}{2},0,\frac{1}{2})$ octahedral interstitial sites which are stable in the α-Fe structure. Since the mechanical milling of powers is generally a non-equilibrium process and almost independent of the milling direction [18], the N atoms also diffuse randomly into the $(\frac{1}{2},\frac{1}{2},0)$ octahedral interstitial site of the a axis with increasing milling time. The result corresponds to the fact that d_{110} and d_{101} gradually become larger with increasing milling time.

However, the martensitic transformation of the Fe_4N–Fe system is difficult to induce in a foil specimen nitrided under the same nitriding conditions [19]. This means that a larger stress is necessary for the stress-induced martensitic transformation in a foil specimen than in a powder specimen, because the atoms in a powder specimen can move easily on applying a small

stress. On the other hand, in the MG process applied to h.c.p. ϵ-Fe_3N no transformation can be detected even after 300 h of milling [20].

5. Conclusions

We have investigated the structural changes and magnetic properties of mechanically milled Fe_4N–4Fe and γ'-Fe_4N alloy powders. In mechanically milled Fe_4N–4Fe and γ'-Fe_4N alloys the γ'-Fe_4N phase is initially transformed into the b.c.t. structure of the α'-Fe type. After 300 h of milling, this martensitic transformation is accomplished in mechanically milled Fe_4N–4Fe powder, but does not reach completion in the mechanical grinding of γ'-Fe_4N.

In the milling process the saturation magnetization (σ) initially increases and the decreases monotonically. The increase in σ is due to the structural change of the γ'-Fe_4N phase from f.c.c. to b.c.t. and the volume expansion of the b.c.t. unit cell. H_c initially increases and becomes almost constant in mechanically alloyed Fe_4N–4Fe, but initially decreases and then becomes constant in the mechanically ground γ'-Fe_4N phase.

On annealing the finally milled Fe_4N–Fe alloys, γ'-Fe_4N is formed above 473 K and α''-$Fe_{16}N_2$ appears together with γ'-Fe_4N above 673 K, causing an increase in σ. However, only α-Fe is retained above 873 K owing to the vaporization of N atoms from the Fe matrix.

Acknowledgments

The authors wish to thank Dr. K. Aoki for his help in the preparation of γ'-Fe_4N. They also acknowledge Dr. K. Takada for his assistance with the ICP analysis. This work was supported financially by a Grant-in-Aid for Scientific Research (03555139 and 03302053) from the Ministry of Education, Science and Culture, Japan.

References

1 M. Komuro, Y. Kozono, M. Hanazo and Y. Sugita, *J. Appl. Phys., 67* (1990) 5126.
2 S.K. Chen, S. Jin, G.W. Kammlott, T.H. Tiefel, D.W. Johnson and E.M. Gyorgy, *J. Magn. Magn. Mater., 110* (1992) 65.
3 Y. Sugita, K. Mitsuoka, M. Komuro, H. Hoshiya, Y. Kozono and M. Hanazono, *J. Appl. Phys., 70* (1991) 1578.
4 H. Kimura, F. Takeda and W.N. Myung, *Mater. Sci. Eng., 97* (1988) 125.
5 S. Surinach, M.D. Baro, J. Segura, M.T. Clavaguera-Mora and N. Clavaguera, *Mater. Sci. Eng. A, 134* (1991) 1368.
6 J. Eckert, L. Schultz and K. Urban, *Appl. Phys. Lett., 55* (1989) 1896.
7 Ch. Kuhrt and L. Schultz, *J. Appl. Phys., 71* (1992) 1896.
8 M.J. Bernal, J.M. Riveiro, A. Hernando, E. Pulido and P. Crespo, *J. Magn. Magn. Mater., 104–107* (1992) 1090.
9 K.J. Kim, H. Onodera, K. Sumiyama and K. Suzuki, *J. Jpn. Soc. Powder Metal., 3* (1993) 303.
10 I. Fall, D.N.C. Uwakweh and J.M.R. Genin, *Hyper. Interact., 69* (1991) 517.
11 V.G. Gavriljuk, V.M. Nadutov and K. Ullakko, *Scr. Metall. Mater., 25* (1991) 905.
12 K.H. Jack, *Proc. R. Soc. A, 208* (1985) 216.
13 H.P. Klug and L.E. Alexander, *X-Ray Diffraction Procedures for Polycrystalline and Amorphous Materials,* Wiley, New York, 1974.
14 K. Mitsuoka, H. Miyajima, H. Ino and S. Chikazumi, *J. Phys. Soc. Jpn., 53* (1984) 2381.
15 Z. Nishiyama, *Martensitic Transformation,* Academic, New York, 1978.
16 G. Shirane, W.J. Takei and S.L. Ruby, *Phys. Rev., 126* (1962) 49.
17 B.C. Frazer, *Phys. Rev., 112* (1958) 751.
18 K.J. Kim, M.S. Es-kandarany, K. Sumiyama and K. Suzuki, *J. Non-Cryst. Solids, 155* (1993) 165.
19 K.J. Kim, K. Sumiyama and K. Suzuki, in preparation.
20 K.J. Kim, K. Sumiyama and K. Suzuki, *J. Phys. Soc. Jap.,* submitted for publication.